Dear Editor and Referee,

Thanks for your suggestions which significantly help us to improve the manuscript. Hereby, we submit our responses and the manuscript has been revised accordingly. If there are any further questions or comments, please let us know.

Best regards

Renzhi Hu on behalf of all co-authors
Key Lab. of Environmental Optics & Technology, Anhui Institute of Optics and Fine Mechanics, Chinese Academy of Sciences
230031 Hefei China
E-mail: rzhu@aiofm.ac.cn

Major Comments

1. ***In section 2, the authors should describe how the OCM and LAM sectors were assigned – by wind direction or trajectory analysis? Some of this description is provided in lines 261 – 270 and I suggest this is moved to section 2.***

Reply:

Thanks for your suggestion. The OCM and LAM sectors were assigned by trajectory analysis. We moved the detailed description to Section 2 (Line 132-140).

Revision:

Line 132-140: Using the hybrid single-particle Lagrangian integrated trajectory (HYSPLIT) model, the 24-h backward trajectories on special days were obtained. In Fig. S1, the red, blue, and green trajectories represent the results at altitudes of 100, 500, and 1000 m above ground level, respectively. Two typical transportation pathways dominated the air parcels. One originated from the northern megacities in the Pearl River Delta (defined as the land mass, LAM), especially on October 18, 19, and 27. In contrast, a clean air mass from the east or northeast was mainly transported to the observation site from the ocean (defined as the ocean mass, OCM), with representative episodes on October 22, 25, and 26.

2. ***Section 2.1: some description of the vegetation type in the surrounding forest should be provided, so the reader can ascertain if other biogenic emissions such as monoterpenes were likely present that could influence the local chemistry.***

Reply:

Thanks for your suggestion. During the observation, the surrounding forest is lush around the YMK site. The vegetation type is evergreen broadleaf forests, which contributed to biogenic emissions. Previous literatures reported the monoterpene concentration in the YMK site, with a daily mean of 0.187 ppb (Zhu et al., 2021). Aboundant biogenic emissions will likely influence the local chemistry. We added the detailed description in Line 120-123.

Revision:

Line 120-123: Previous literatures reported the monoterpene concentration in the YMK site, with a daily mean of 0.187 ppb (Zhu et al., 2021). Aboundant biogenic emissions will likely influence the local chemistry.

3. *Line 132: '..via chemical transformation' add 'by addition of NO'. Please also state the purity of the NO and concentration of NO in the detection cell.*

Reply:

Thanks for your suggestion. The purity of the NO was mixed with 2% in N_2, and the concentration of NO in the detection cell was ~1.6×10^{12} cm^{-3}. NO was passed through a ferrous sulfate filter to remove impurities (NO_2, HONO, and so on) before being injected into the detection cell. We added the detailed description in Line 187-195.

Revision:

Line 187-195: For HO_2 measurement, the NO gas was mixed with 2% in N_2 to achieve HO_2-to-OH conversion. NO was passed through a ferrous sulfate filter to remove impurities (NO_2, HONO, and so on) before being injected into the detection cell. The NO concentration (~1.6×10^{12} cm^{-3}) corresponding to a conversion efficiency of ~15% was selected to avoid $RO_2 \rightarrow HO_2$ interference (especially from RO_2 radicals derived from long-chain alkanes (C ≥ 3), alkenes, and aromatic hydrocarbons). Previous study denoted that the percentage interference from alkene-derived RO_2 under these operating conditions was no more than 5% (Wang et al., 2021).

4. *Line 147: Is this a single pass laser configuration or multi-pass? Please state*

Reply:

Thanks for your suggestion. The radical detection module utilized a single pass laser configuration, and the laser beam was amplified to a diameter of 8 mm. We stated the detailed description in Line 158-160.

Revision:

Line 158-160: The radical detection module utilized a single pass laser configuration,

and the laser beam was amplified to a diameter of 8 mm.

5. *Line 155: change 'avoid' to 'reduce'*

Reply:

We followed the reviewer's comment. We changed the description in Line 167-170.

Revision:

Line 167-170: Efficient ambient air sampling was achieved using an aluminum nozzle (0.4 mm orifice), and the pressure in the chamber was maintained at 400 Pa via a vortex vacuum pump (XDS35i, Edwards) to reduce fluorescence quenching.

6. *Line 159: The ozone interference as a function of ambient ozone and H_2O (v) concentration and laser power determined from the laboratory experiment should be provided.*

Reply:

Thanks for your suggestion. We added the detailed description in Line 173-177.

Revision:

Line 173-177: Due to the synchronous reaction at 308nm, wavelength modulation is not applicable to ozone photolysis interference. Through laboratory experiments, at 20 mW laser energy, every 1% water vapor concentration and 50 ppb ozone concentration can generate a 2.5 × 10^5 cm^{-3} OH concentration. The results in this paper have subtracted the ozone photolysis interference (Fig. S2).

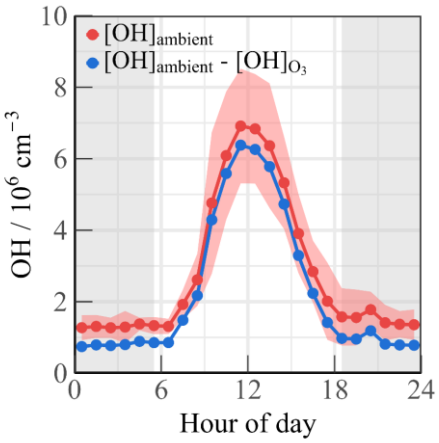

Fig. S2. Mean diurnal profiles of measured [OH] before (red line) and after (blue line) deducting the O_3

interference. The coloured shadows denote the 25 and 75% percentiles. The grey areas denote nighttime.

7. ***Line 160 -164: The previous good agreement reported for OH measurements by this system and the PKU-LIF in a previous study doesn't translate to an interference-free OH observation in the present study. Chemical removal of ambient OH using an inlet pre-injector is now seen as standard practice for LIF OH instruments. In the absence of this, the authors should provide some information on the chemical environment (ozone, alkene, NOx concentrations) were the instrument was deployed during the intercomparison and explain how this contrasts with the current environmental conditions.***

Reply:

Thanks for your suggestion. We will discuss whether internal interference exists in AIOFM-LIF from the following aspects:

First of all, literature research shows that measurement interference is more related to the length of the inlet in the low-pressure cell (Griffith et al., 2016). In terms of system design, the AIOFM-LIF system uses a short-length inlet design to minimize this and other unknown disturbances (The distance from radical sampling to fluorescence excitation is ~150 mm).

Additionally, potential interference may exist when the atmosphere contains abundant alkenes, ozone, and BVOCs, indicating that environmental conditions play leading roles in OH interferences (Mao et al., 2010; Fuchs et al., 2016; Novelli et al., 2014). An OH measurement comparison with a LIF instrument deployed an inlet pre-injector (PKU-LIF), was conducted in a real atmosphere in a previous study (Zhang et al., 2022). The ozonolysis interference on the measurement consistency of both systems was excluded under high-VOCs conditions. We have compared the chemical conditions during the intercomparison experiment and the current environmental conditions. Overall, the key parameters related to ozonolysis reactions (O_3、alkenes、isoprene and NOx) in YMK were similar to those during the comparison experiment, which is not conducive to generating potential OH interference. Therefore, it is not expected that OH measurement in the present study was affected by internal interference. We added

the detailed description in Line 177-187.

Table.S1. Comparison of key parameters related to ozonolysis reactions (O_3、alkenes、isoprene and NOx) between YMK and the intercomparison experiment. All the values are the diurnal average (10:00-15:00).

Species	Intercomparison	YMK
O_3 (ppb)	71.02	74.58
Alkenes (ppb)	1.29	1.10
Isoprene (ppb)	0.67	0.64
NOx (ppb)	5.65	4.24

Revision:

Line 177-187: In terms of system design, the AIOFM-LIF system incorporates a short-length inlet design to minimize interferences from ozonolysis and other unknown factors (the distance from radical sampling to flourescence excitation is ~150 mm). An OH measurement comparison with an interference-free instrument, PKU-LIF, was conducted in a real atmosphere in a previous study (Zhang et al., 2022). The ozonolysis interference on the measurement consistency of both systems was excluded under high-VOCs condition. Overall, the key parameters related to ozonolysis reactions (O_3、alkenes、isoprene and NOx) in YMK was similar to that during the intercomparison experiment, implies that the chemical conditions do not favor the generation of potential interference to OH measurement (Table S1).

8. Line 166: The authors need to state the percentage interference from an alkene-derived RO2 under these operating conditions (it won't be zero).

Reply:

Thanks for your suggestion. In the previous work, we have calculated the conversion efficiency of alkene-derived RO_2 to OH under different NO concentration (Wang et al., 2021). In the YMK observation, ethene accounted for about 70% of the total ethene concentration (Table S5). Therefore, we choose ethene and isoprene to investigate the percentage interference from an alkene-derived RO_2. When NO was at 1.6×10^{12} cm^{-3}, the conversion efficiency of HO_2 was ~15%, and the percentage

interference from ethene and isoprene-derived RO_2 was 3.83% and 1.75%, respectively (Wang et al., 2021). We added the detailed description in Line 193-195.

Revision:

Line 193-195: Previous study denoted that the percentage interference from alkene-derived RO_2 under these operating conditions was no more than 5% (Wang et al., 2021).

9. Line 169: How much OH and HO2 was produced in the calibration? Was the calibration performed using a turbulent flow? How was the lamp flux determined? These details should be included in the manuscript.

Reply:

Thanks for your suggestion. In the YMK observation, the calibration was performed in a laminar condition with a maximum flow rate of 20 SLM (standard liters per minute)(Wang et al., 2020; Wang et al., 2019). OH concentration was deduced by chemical radiometry according to the next Eq. :

$$[OH] = [HO_2] = \frac{1}{2} \cdot \frac{\sigma_{H_2O}}{\sigma_{O_2}} \cdot \frac{[H_2O]}{[O_2]} \cdot \frac{[O_3]}{P}$$

σ_{H_2O} and σ_{O_2} represent the absorption cross-sections of water and oxygen, respectively. P represents the distribution factor of ozone concentration inside the tube. In previous studies, we obtained the actual measured values of σ_{O_2} and P through experiments (Wang et al., 2020). As the luminous flux in photolysis region is difficult to accurately measure, the linearly correlation between ozone concentration and 185 nm light flux was established. Ozone concentration in the flow tube was measured by a home-made Cavity Ring Down Spectrometer (CRDS, and the detection limit is 15 ppt@30 s, 1σ). Mercury lamp intensity is adjusted to establish.

In the YMK campaign, the humidity varied between 40 – 80% (Fig. S3). In order to test different atmospheric conditions, both low (~40%) and high (~70%) levels of water vapor were selected to produce OH and HO_2 radicals for calibration, and the corresponding HOx concentration obtained from the standard source was 1.0×10^9 cm^{-3} and 1.8×10^9 cm^{-3}, respectively (Zhang et al., 2022).

We added the detailed description in Line 196-212.

Revision:

Line 196-212: A standard HOx radical source was used to complete the calibration of the detection sensitivity (Wang et al., 2020). The radical source is based on the simultaneous photolysis of H_2O/O_2 by a 185 nm mercury lamp. Humidified air flow is introduced to produce equal amounts of OH and HO_2 radicals after passing the photolysis region. The flow remained in a laminar condition with a maximum flow rate of 20 SLM (standard liters per minute). As the luminous flux in photolysis region is difficult to accurately measure, the linearly correlation between ozone concentration and 185 nm light flux was established. Ozone concentration in the flow tube was measured by a home-made Cavity Ring Down Spectrometer (CRDS, and the detection limit is 15 ppt@30 s, 1σ). Mercury lamp intensity is adjusted to establish. The instrument was calibrated every 1 or 2 days (except for shutdown during rainy periods), and the sensitivity used for the data processing was an average of all of the calibration results. In the YMK campaign, the humidity varied between 40 – 80% (Fig. S3). In order to test different atmospheric conditions, both low (~40%) and high (~70%) levels of water vapor were selected to produce OH and HO_2 radicals for calibration, and the corresponding HOx concentration obtained from the standard source was 1.0×10^9 cm^{-3} and 1.8×10^9 cm^{-3}, respectively (Zhang et al., 2022).

10. Section 2.2.2: Given the importance of HONO as an OH source in this study, some comments on possible instrument artefacts/or how interferences were corrected for should be discussed.

Reply:

Thank you for your suggestion. HONO measurement was conducted using a commercial Long-Path Absorption Photometer (LOPAP). The LOPAP method utilizes two absorption tubes in series for differential correction, which effectively eliminates the influence of known interfering substances such as NO_2 and N_2O_5, offering an advantage over traditional wet chemistry methods. This method has been extensively tested for its suitability in detecting HONO in complex atmospheric conditions, as

demonstrated in previous studies by(Yang et al., 2022a; Yang et al., 2021b; Wang et al., 2023). During the YMK campaign, zero air measurements were taken every 8 hours for a duration of 20 minutes to correct for instrument baseline fluctuations. Additionally, a liquid nitrite standard calibration was performed on a weekly basis to ensure the accuracy of the calibration curve used for measuring HONO concentrations. We added the detailed description in Line 225-233.

Revision:

Line 225-233: HONO measurement was conducted using a commercial Long-Path Absorption Photometer (LOPAP). The LOPAP method utilizes two absorption tubes in series for differential correction, which effectively eliminates the influence of known interfering substances such as NO_2 and N_2O_5, offering an advantage over traditional wet chemistry methods. Zero air measurements were taken every 8 hours for a duration of 20 minutes to correct for instrument baseline fluctuations. This method has been extensively tested for its suitability in detecting HONO in complex atmospheric conditions, as demonstrated in previous studies by (Yang et al., 2022a; Yang et al., 2021b; Wang et al., 2023).

11. Line 183: Which of the measured photolysis rates were used as model constraints?

Reply:

Thanks for your suggestion. Eight measured photolysis rates ($j(NO_2)$, $j(H_2O_2)$, j(HCHO), j(HONO), $j(NO_2)$, $j(NO_3)$, $j(O^1D)$) were used as model constraints.

Revision:

Line 233-234: Eight measured photolysis rates ($j(NO_2)$, $j(H_2O_2)$, j(HCHO), j(HONO), $j(NO_2)$, $j(NO_3)$, $j(O^1D)$) were used as model constraints.

12. Line 204: Did the modelled OH and HO2 reach a steady state concentration during this time – what was the % difference between day 2 and day 3 radical concentrations?

Reply:

We followed the reviewer's comment. We calculated the steady state concentrations of OH and HO_2 radical using the Eq.(1)(2):

$$[OH]_{PSS} = \frac{j_{HONO}[HONO] + \varphi_{OH} j(O^1D)[O_3] + k_{HO_2+NO}[NO][HO_2]}{k_{OH}} \quad (1)$$

$$[HO_2]_{PSS} = \frac{k_{CO+OH}[CO][OH] + j_{HCHO}[HCHO] + k_{RO_2+NO}[NO][RO_2]}{k_{HO_2+NO}[NO]} \quad (2)$$

Due to the lack of RO_2 radical observation data, substitute the $[RO_2]$ and k_{OH} items in Eq.(1)(2) with the simulated value. The comparison of steady state and the modelled concentrations in the daytime were shown in Fig.3. During the entire observation period, the base model reached a steady state and showed good agreement with the calculated concentrations of OH and HO_2 radicals using Eq.(1)(2). Specifically, on the second and third days, there were no significant differences between the steady-state calculation and the base model, with OH and HO_2 concentration deviations of 7.5% and 3.1%, respectively.

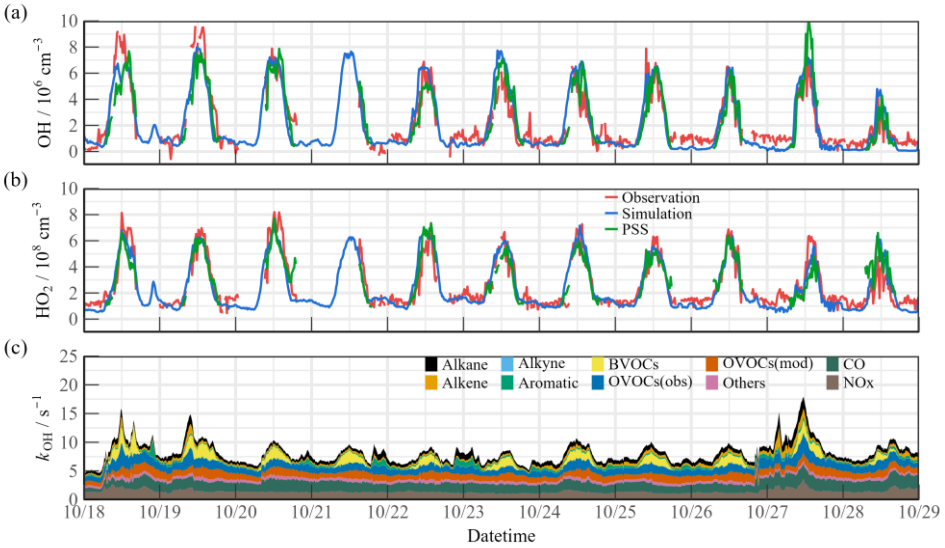

Fig. 3. Timeseries of the observed and modelled parameters for OH, HO_2 and k_{OH} during the observation period. **(a)** OH, **(b)** HO_2, **(c)** k_{OH}.

Revision:

Line 262-267: In addition, another steady-state calculation method (PSS) can also be used to estimate the concentrations of OH and HO_2 radicals (Eq. (1)(2), (Woodward-Massey et al., 2022; Slater et al., 2020)). Since the k_{OH} and RO_2 concentrations were not obtained in this observation, simulated values are used as substitutes. Other radical and reactive intermediates are actual values that measured from the instruments in Table S2.

Line 369-374: Overall, the observed OH and HO_2 concentrations were both well reproduced by the base model incorporating the RACM2-LIM1 mechanism. The observed OH was underestimated only on the first days, and a slight model overestimation happened on October 23&24. PSS calculation showed good agreement with the base model, providing evidence of the balance of radical internal consistency in the daytime.

13. Line 208: Could the authors explain their choice of the 18 hr lifetime? Were any model tests performed to assess how well the model predicted HCHO for example (if left unconstrained to HCHO) with an 18 hr lifetime? How sensitive were the modelled OH, HO2 and modelled kOH to the choice of this lifetime?

Reply:

Thanks for your suggestion. After literature research, we found that the lifetime for the model-generated intermediate is usually set between 8 – 24 h (Ma et al., 2022; Yang et al., 2021a; Whalley et al., 2021). We tested the relationship between the first-order loss term and simulated OH, HO_2, k_{OH} by changeing the lifetime (8h, 12h, 18h, and 24h). The results have been added to Fig. S4. The sensitivity analysis shows that when the lifetime changes within 8 – 24 hours (8h, 12h, 18h, and 24h). The values differed less than 5% between two cases for both OH, HO_2, k_{OH}. Therefore, we finally chose a settling time of 18 hours, corresponding to first order loss rate of ~1.5 cm/s (by assuming a boundary layer height of about 1 km).

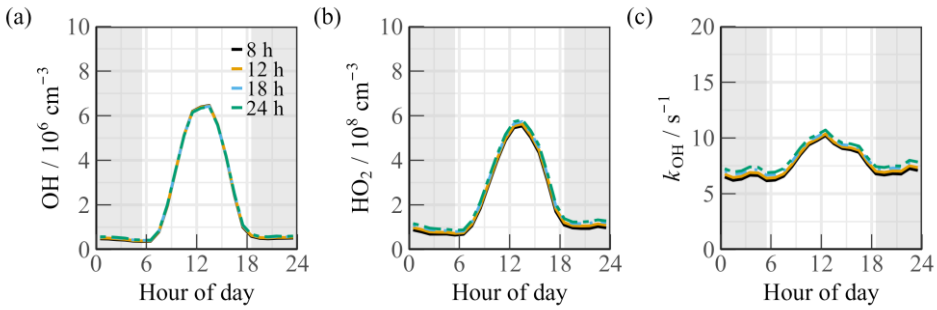

Fig. S4. The relationship between the first-order loss term and simulated **(a)** OH, **(b)** HO_2, **(c)** k_{OH} by changeing the lifetime within 8 – 24 hours (8h, 12h, 18h, and 24h).

To test the sensitivity of the HCHO simulation, data from October 18th to 22nd were selected (in the Figure below). The study found that when the lifetime was altered

between 8 and 24 hours, the simulated HCHO concentrations changed in a manner consistent with the observed values from the YMK site. However, the model tended to overestimate formaldehyde concentrations over longer time periods. This phenomenon of overestimation has been found in other areas as well (Li et al., 2014).

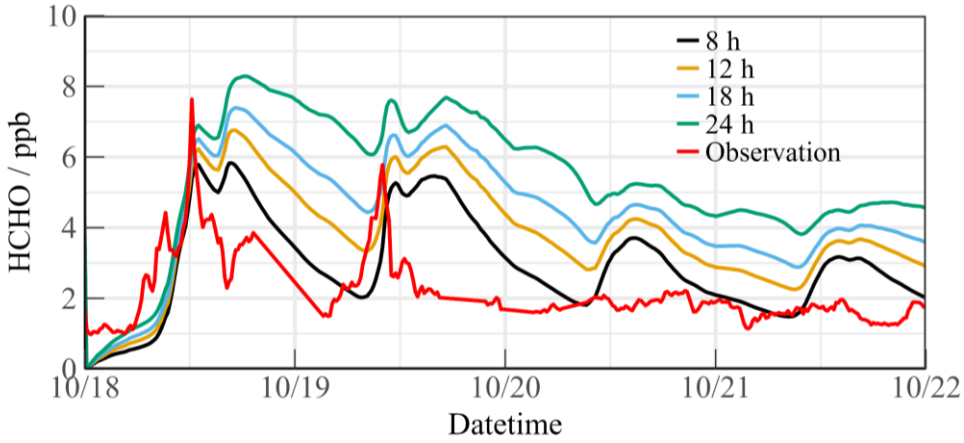

We added the detailed description in Line 255-260.

Revision:

Line 255-260: The physical losses of species due to processes such as deposition, convection, and advection were approximately replaced by an 18 h atmospheric lifetime, corresponding to first order loss rate of ~1.5 cm/s (by assuming a boundary layer height of about 1 km). The sensitivity analysis shows that when the lifetime changes within 8 – 24 hours, the values differed less than 5% for both OH, HO_2, k_{OH} (Fig. S4).

14. Line 211 – 217: What was the modelled BrO concentration when the model was run with Br2 chemistry? I think some comment on the potential impact of iodine chemistry should be included in this section (as other papers which focus on the chemistry of the marine boundary layer consider both iodine and bromine chemistry). With regards to the Tables S2 and S3 provided in the SI, what are the expected products from the photolysis reactions in S2? HOBr photolysis is a source of OH, was this included as the photolysis product in the model? For S3, 'ACD' and 'MO2' need defining. Were heterogeneous loss processes for HOBr considered? In Bloss et al., ACP, 2010, the reaction of CH3O2 + BrO produces HOBr + CH2O2 (which dissociates to CO and H2O). Could the authors

explain/provide a reference for their choice of products (HOBr, HO2 and HCHO) from this reaction? As it is written, the reactants and products don't balance. As it stands, the halogen scheme included seems incomplete and I suggest this is reviewed before final publication.

Reply:

In the previous manuscript, when the model was run with Br_2 chemistry, the diurnal concentration of BrO was depicted in the following Figure. During the observation period, BrO concentration exhibited a clear diurnal variation with peak concentrations at 0.68 ppt. This value is consistent with the simulated results observed by HZ (~0.5 ppt) but lower than those obtained at CHABLIS (~5.0 ppt) (Bloss et al., 2010; Xia et al., 2022).

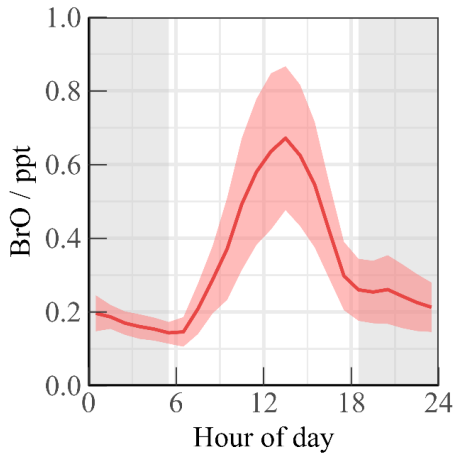

Some deficiencies of Tables S3 and S4 were identified in the previous manuscript version, which have now been addressed. Iodine-related mechanisms are also considered, and the photolysis products in Table S3 have been added, including the photolysis of HOBr (the uptake process of HOBr was not considered). ACD and ACO_3 represent Acetaldehyde and Acetyl peroxy radicals, respectively, in the RACM2 mechanism. Meanwhile, MO_2 represents Methyl peroxy radicals. Explanations for ACD, ACO_3 and MO_2 have also been added to the table notes in Table S4. Additionally, we agree with the authors' suggestion that the subsequent decomposition products of CH_3O_2 + BrO actually yield HOBr + CO + H_2O instead of HOBr + HO_2 + HCHO.

In order to better explore the effect of Br and I chemistry on HOx radicals, we

chose BrO/IO as the initiation point of halogen chemistry in the latest version of the manuscript. The concentration of BrO and IO is set to ~5 ppt, which is a typical level in MBL site (Xia et al., 2022; Bloss et al., 2010; Whalley et al., 2010). In this scenario (Fig. 4, green line). The daytime concentration of HO_2 radical decreased by 8.5% and 13.3% during the LAM and OCM periods, respectively, compared to the base model. However, there was no significant change in the concentration of OH radicals (<3%).

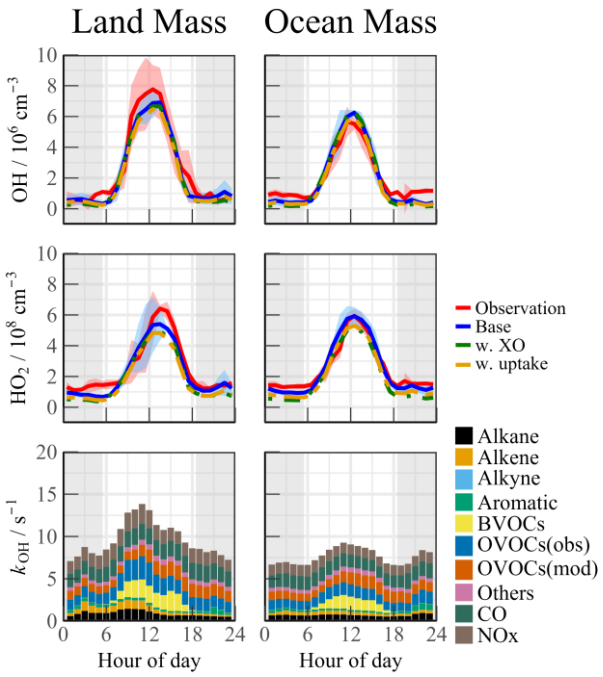

Fig. 4. Median diurnal profiles of the observed and modelled OH, HO_2, k_{OH} during LAM and OCM episodes. The coloured shadows for OH and HO_2 radicals denote the 25 and 75% percentiles. The grey areas denote nighttime.

We added the detailed description in Line 417-426.

Revision:

Line 417-426: Halogen species have been recognized as potent oxidizers that can boost photochemistry (Xia et al., 2022; Peng et al., 2021). A sensitivity test was performed by imposing BrO and IO into the base model to diagnose the impact of the halogen chemistry on the troposphere chemistry. The concentration of BrO and IO is set to ~5 ppt, which is a typical level in MBL site (Xia et al., 2022; Bloss et al., 2010; Whalley et al., 2010). The details of the mechanisms involved are listed in Tables S3 and S4. In this scenario (Fig. 4, green line). The daytime concentration of HO_2 radical decreased by 8.5% and 13.3% during the LAM and OCM periods, respectively, compared to the

base model. However, there was no significant change in the concentration of OH radicals (<3%).

Table S3-S4:

Table.S3. Photolysis frequencies for Br-related species (Atkinson et al., 2007; Bloss et al., 2010).

Reaction	Mean j(x) / j(NO_2)	References
Br_2 + *hv*--> Br+Br	3.45	(Atkinson et al., 2007)
BrO + *hv*--> Br+O	5.41	(Atkinson et al., 2007)
$BrONO_2$--> Br + NO_3	0.16	(Atkinson et al., 2007)
BrONO + *hv*--> Br + NO_2	1.14	(Atkinson et al., 2007)
BrONO + *hv*--> BrO + NO	1.14	(Atkinson et al., 2007)
HOBr + *hv*--> Br + OH	0.256	(Atkinson et al., 2007)
I_2 + *hv*--> I + I	20.30	(Atkinson et al., 2007)
IO+ *hv*--> I + O	18.30	(Bloss et al., 2001)
OIO + *hv*--> I + O_2	2.58	(Cox et al., 1999)
$IONO_2$ + *hv*--> I + NO_3	0.556	(Joseph et al., 2007)
I_2O_2 + *hv*--> IO + IO	0.556	(Joseph et al., 2007)
I_2O_3 + *hv*--> IO + OIO	0.556	(Joseph et al., 2007)
I_2O_4 + *hv*--> OIO + OIO	0.556	(Joseph et al., 2007)
INO_2 + *hv*--> I +NO_2	0.319	(Bloss et al., 2010)
INO + *hv*--> I + NO	3.71	(Bloss et al., 2010)
HOI + *hv*--> OH + I	1.12	(Atkinson et al., 2007)

Table.S4. Gas-phase kinetics for Br-related species in RACM2 mechanism. Revised by (Bloss et al., 2010). ACD and ACO_3 represent Acetaldehyde and Acetyl peroxy radicals, respectively, in the RACM2 mechanism. Meanwhile, MO_2 represents Methyl peroxy radicals. PI_1, PI_2, PI_3, PI_4 are the particulate iodine.

Reaction	Reaction rate constant (cm^3s^{-1})	References
Br + O_3 --> BrO + O_2	$1.7 \times 10^{-11}\exp(-800/T)$	(Atkinson et al., 2007)
Br + HO_2 --> HBr + O_2	$7.7 \times 10^{-12}\exp(-450/T)$	(Atkinson et al., 2007)
HBr + OH --> Br + H_2O	$6.7 \times 10^{-12}\exp(155/T)$	(Atkinson et al., 2007)
Br_2 + OH --> HOBr + Br	$2.0 \times 10^{-11}\exp(240/T)$	(Atkinson et al., 2007)
Br + HCHO --> HBr + HCO	$7.7 \times 10^{-12}\exp(-580/T)$	(Atkinson et al., 2007)
Br + ACD --> HBr + ACO_3	$1.8 \times 10^{-11}\exp(-460/T)$	(Atkinson et al., 2007)
Br + NO_2 --> BrONO	$k_0 = 4.2 \times 10^{-31}\exp(T/300)^{-2.4}$ $k_\infty = 2.7 \times 10^{-11}$, $F_c = 0.6$	(Bloss et al., 2010)
BrO + BrO --> Br + Br + O_2	2.7×10^{-12}	(Atkinson et al., 2007)
BrO + BrO --> Br_2 + O_2	$2.9 \times 10^{-14}\exp(840/T)$	(Atkinson et al., 2007)
BrO + HO_2 --> HOBr + O_2	$4.5 \times 10^{-12}\exp(500/T)$	(Atkinson et al., 2007)
HO + HOBr --> BrO + H_2O	5.0×10^{-11}	(Bloss et al., 2010)
BrO + MO_2 --> HOBr+ CO + H_2O	$4.6 \times 10^{-13}\exp(798/T)$	(Enami et al., 2007)
BrO + NO --> Br + NO_2	$8.7 \times 10^{-12}\exp(260/T)$	(Atkinson et al., 2007)
BrO + NO_2 --> $BrONO_2$	$k_0 = 5.2 \times 10^{-31}\exp(T/300)^{-3.2}$ $k_\infty = 6.9 \times 10^{-12}\exp(T/300)^{-2.9}$, $F_c = 0.6$	(Bloss et al., 2010)
$BrONO_2$ --> BrO + NO_2	$2.8 \times 10^{13}\exp(12360/T)$	(Orlando and Tyndall, 1996)
I + O_3 --> IO + O_2	$k = 2.1 \times 10^{-11}\exp(-830/T)$	(Atkinson et al., 2007)
I + HO_2 -->HI + O_2	$k = 1.5 \times 10^{-11}\exp(-1090/T)$	(Atkinson et al., 2007)
OH + HI -->I + H_2O	$k = 1.6 \times 10^{-11}\exp(440/T)$	(Atkinson et al., 2007)
OH + I_2 -->HOI + I	$k = 2.1 \times 10^{-10}$	(Atkinson et al., 2007)
NO_3 + I_2 --> I + $IONO_2$	$k = 1.5 \times 10^{-12}$	(Atkinson et al., 2007)

$NO_3 + HI \rightarrow HNO_3 + I$	$k = 1.3 \times 10^{-12}\exp(-1830/T)$	(Atkinson et al., 2007)
$I + NO_2 \rightarrow INO_2$	$k_0 = 3.0 \times 10^{-31}(T/300)^{-1.0}$ $k_\infty = 6.6 \times 10^{-11}$, $F_c = 0.6$	(Bloss et al., 2010)
$INO_2 \rightarrow I + NO_2$	$k = 0.14\ s^{-1}$ (at 268 K)	(Bloss et al., 2010)
$INO_2 + INO_2 \rightarrow I_2 + 2NO_2$	$k = 4.7 \times 10^{-13}\exp(-1670/T)$	(Atkinson et al., 2007)
$I + NO \rightarrow INO$	$k_0 = 1.8 \times 10^{-32}(T/300)^{-1.0}$ $k_\infty = 1.7 \times 10^{-11}$, $F_c = 0.6$	(Bloss et al., 2010)
$INO \rightarrow I + NO$	$k = 0.087\ s^{-1}$ (at 268 K)	(Bloss et al., 2010)
$INO + INO \rightarrow I_2 + NO + NO$	$k = 8.4 \times 10^{-11}\exp(-2620/T)$	(Atkinson et al., 2007)
$IO + IO \rightarrow 2I + O_2$	$k = 0.11 \times 5.4 \times 10^{-11}\exp(180/T)$	(Atkinson et al., 2007)
$IO + IO \rightarrow I + OIO$	$k = 0.38 \times 5.4 \times 10^{-11}\exp(180/T)$	(Atkinson et al., 2007)
$IO + IO \rightarrow I_2O_2$	$k = 0.51 \times 5.4 \times 10^{-11}\exp(180/T)$	(Atkinson et al., 2007)
$IO + HO_2 \rightarrow HOI + O_2$	$k = 1.4 \times 10^{-1}1\exp(540/T)$	(Atkinson et al., 2007)
$OH + HOI \rightarrow IO + H_2O$	$k = 1.0 \times 10^{-10}$	(Dillon et al., 2006)
$IO + CH_3O_2 \rightarrow CH_3O + IOO$	$k = 2.0 \times 10^{-12}$	(Dillon et al., 2006)
$IO + NO \rightarrow I + NO_2$	$k = 7.15 \times 10^{-12}\exp(300/T)$	(Atkinson et al., 2007)
$IO + NO_2 \rightarrow IONO_2$	$k_0 = 6.5 \times 10^{-31}(T/300)^{-3.5}$ $k_\infty = 7.6 \times 10^{-12}(T/300)^{-1.5}$, $F_c = 0.6$	(Bloss et al., 2010)
$IONO_2 \rightarrow IO + NO_2$	$k = 2.1 \times 10^{15}\exp(-13670/T)$	(Kaltsoyannis and Plane, 2008)
$IO + NO_3 \rightarrow OIO + NO_2$	$k = 9.0 \times 10^{-12}$	(Dillon et al., 2006)
$I + NO_3 \rightarrow IO + NO_2$	$k = 1.0 \times 10^{-12}$	(Dillon et al., 2006)
$IO + BrO \rightarrow I + Br + O_2$	$k = 0.2 \times 1.5 \times 10^{-11}\exp(510/T)$	(Atkinson et al., 2007)
$IO + BrO \rightarrow Br + OIO$	$k = 0.8 \times 1.5 \times 10^{-11}\exp(510/T)$	(Atkinson et al., 2007)
$IO + OIO \rightarrow I_2O_3$	$k = 5 \times 10^{-11}$	(Martin et al., 2009)
$OIO + OIO \rightarrow I_2O_4$	$k = 1.5 \times 10^{-10}$	(Martin et al., 2009)
$OIO + I_2O_3 \rightarrow PI_1$	$k = 1.5 \times 10^{-10}$	(Martin et al., 2009)
$OIO + I_2O_4 \rightarrow PI_2$	$k = 1.5 \times 10^{-10}$	(Martin et al., 2009)
$I_2O_2 + O_3 \rightarrow I_2O_3 + O_2$	$k = 1.0 \times 10^{-12}$	(Saunders and Plane, 2005)
$I_2O_3 + O_3 \rightarrow I_2O_4 + O_2$	$k = 1.0 \times 10^{-12}$	(Saunders and Plane, 2005)
$I_2O_4 + O_3 \rightarrow PI_3$	$k = 1.0 \times 10^{-12}$	(Saunders and Plane, 2005)
$I_2O_2 \rightarrow IO + IO$	$k = 10.0\ s^{-1}$	(Kaltsoyannis and Plane, 2008)
$I_2O_4 \rightarrow OIO + OIO$	$k = 0.1\ s^{-1}$	(Kaltsoyannis and Plane, 2008)
$NO + OIO \rightarrow IO + NO_2$	$k = 1.1 \times 10^{-12}\exp(542/T)$	(Plane et al., 2006)
$OH + OIO \rightarrow PI_4(HIO_3)$	$k = 2.2 \times 10^{-10}\exp(243/T)$	(Plane et al., 2006)
$BrO + DMS \rightarrow Br + DMSO$	$k = 1.4 \times 10^{-14}\exp(950/T)$	(Bloss et al., 2010)
$Br + DMS \rightarrow HBr + CH_3SCH_2$	$k = 9.0 \times 10^{-11}\exp(-2390/T)$	(Bloss et al., 2010)
$IO + DMS \rightarrow I + DMSO$	$k = 1.2 \times 10^{-14}$	(Bloss et al., 2010)

15. Line 233: 'exhibited good consistency..' it would be useful to provide typical concentrations of CO and PM2.5 to aid comparison to the previous campaigns referenced.

Reply:

Thanks for your suggestion. We have added the range of CO and $PM_{2.5}$ concentrations in Line 326-328.

Revision:

Line 326-328: The CO and $PM_{2.5}$ concentrations exhibited good consistency and even mild pollution features ((0.36 ± 0.12 ppm) and (37.70 ± 7.91 μg/m^3), respectively),

reflecting the influence of human activities.

16. Section 3.1.1: As the paper is trying to contrast LAM and OCM sectors, I think it would be useful from the start of this section to provide concentrations for the species discussed (e.g. NMHCs, NOx, CO, O3) from both sectors rather than campaign averages.

Reply:

Thanks for your suggestion. We have modified the Section to provide concentrations for the species discussed (e.g. NMHCs, NOx, CO, O_3) from both sectors rather than campaign averages.

Revision:

Line 301-351:

As typical marine air components, the concentrations of NOx, CO, $PM_{2.5}$, and other pollutants were lower than those detected in other observation campaigns in both urban and suburban areas in the Pearl River Delta region (Tan et al., 2019; Lu et al., 2012; Yang et al., 2022b). Serval observation campaigns have discovered the relationship between wind direction and radical chemistry (Lu et al., 2012; Fuchs et al., 2017; Niu et al., 2022). Although there was no apparent wind speed condition, the dominant air mass still influenced the pollutant concentrations due to the particularity of the marine site.

During the OCM period, the NOx and HCHO concentrations exhibited relatively clean characteristics that were consistent with those previously observations in open ocean (RHaMBLe, SOS, CHABLIS and ALBATROSS, Table 1). Isoprene, a representative BVOC, achieved a diurnal concentration of 0.58 ± 0.06 ppb, indicated slightly local emissions could have impacted the concentrations of the precursor species even in OCM sector. The ozone concentration in the YMK site was always at the critical value of the updated Class I standard (GB3095-2012, average hourly O_3 of 81 ppb at 25°C and 1013 kPa). The occurrence of fewer emissions reduced the titration effect, resulting in the ozone exhibiting no apparent diurnal trend on some of the dates and a

high background value at night (78.1 ± 7.6 ppb).

As a coastal site, chemical conditions could be influenced by local land emissions depending on the wind direction. Compared with the OCM period, the meteorological conditions (T, RH, and J-values) changed slightly during the LAM episode, but the pollutants were accumulated due to the transport of the plume from the northern cities (Fig. 2). The CO and $PM_{2.5}$ concentrations exhibited good consistency and even mild pollution features ((0.36 ± 0.12 ppm) and (37.70 ± 7.91 μg/m^3), respectively), reflecting the influence of human activities. Both NO and NO_2 peaked at around 10:00, exhibiting prominent pollution characteristics. HONO exhibited a distribution with high daytime (0.66 ± 0.08 ppb) and low nighttime (0.33 ± 0.09 ppb) concentrations. This unique distribution of HONO has been observed in remote environments in several previous observation campaigns (Jiang et al., 2022; Crilley et al., 2021). High HONO concentration in the daytime will affect the chemical composition of the atmosphere and the secondary pollution generation.

The detailed information for VOCs species during the YMK campaign has been added in the Table S5. The daily maximum NMHC concentration peaked at 27.81 ± 9.91 ppb, and the maximum value of ~40 ppb occurred on October 27. Local biological emissions significantly affected the NMHC composition of the site, and isoprene achieved a noon maximum of 0.82 ± 0.16 ppb. Neither anthropogenic alkenes (2.21 ± 0.94 ppb) nor aromatic (1.31 ± 0.25 ppb) hydrocarbons were abundant, and OVOCs accounted for approximately 50% of the total. As a photochemical indicator, formaldehyde peaked at ~4 to ~8 ppb during the LAM episode, suggesting a more vigorous oxidation process. The HONO concentration was 6.8 times higher than the SW scenario in the ICOZA observation (a pollution period dominated by a southwest wind direction), while the HCHO concentration was 3.1 times higher. (Woodward-Massey et al., 2022). The abundance of oxidation precursors (HONO, HCHO, O_3, and NMHCs) reflected the unique atmospheric conditions in the marine environment in China, which originated from the complex atmospheric pollution.

17. Line 235: I don't think it is 'conventional belief' that marine ozone would

necessarily be at background levels. At coastal sites which are influenced by land emissions, as is the case at the YMK site, I don't think it is unexpected to observe net ozone production given the NOx concentrations reported. I think it would be valuable to highlight, perhaps in Table 1, contrasting marine environments – for example, some of the referenced literature are from marine sites which are considered representative of the open ocean (RHaMBLe, SOS, ALBATROSS), whereas others, including YMK, are coastal sites which, depending on the wind direction, could be influenced by local land emissions.

Reply:

Thanks for your suggestion. We adopted the suggestions of reviewers and marked the types of ocean observations in Table1. Three of the observations by RHaMBLe, SOS, and ALBATROSS were classified as open ocean, while the others were considered coastal features. We have also made some changes in the manuscript (Line 312-314&322-323).

Revision:

Line 312-314: During the OCM period, the NOx and HCHO concentrations exhibited relatively clean characteristics that were consistent with those previously observations in open ocean (RHaMBLe, SOS, CHABLIS and ALBATROSS, Table 1).

Line 322-323: As a coastal site, chemical conditions could be influenced by local land emissions depending on the wind direction.

18. Line 246: provide typical concentrations of alkenes and aromatics.

Reply:

Thanks for your suggestion. We have added the typical concentrations of alkenes and aromatics during the daytime (10:00 – 15:00). The detailed information table for VOCs species during the YMK campaign has been added in the Table S5.

Revision:

Line 342-344: Neither anthropogenic alkenes (2.21 ± 0.94 ppb) nor aromatic (1.31 ± 0.25 ppb) hydrocarbons were abundant, and OVOCs accounted for approximately 50%

of the total.

Table. S5. The detailed information table for VOCs species during the YMK campaign. The mean concentration, standard deviation (SD), minimum value (Min), maximum value (Max), and percentage contribution in the species for the top-five ranked species in alkanes, alkenes, aromatic and OVOCs are listed. All the values are the daily average (0:00-24:00).

Species	Mean (ppb)	Sd (ppb)	Min (ppb)	Max (ppb)	Proportion (%)
Alkane					
ethane	1.72	0.564	0.24	5.621	29.2
propane	1.246	0.524	0.136	5.438	21.15
n-butane	0.646	0.395	0.054	2.424	10.97
i-butane	0.561	0.471	0.029	3.372	9.52
n-hexane	0.41	0.307	0.033	3.026	6.96
Alkene					
ethene	0.592	0.656	0.034	5.48	69.08
propene	0.123	0.127	0.017	1.187	14.35
1-butene	0.046	0.014	0.012	0.107	5.37
trans-2-butene	0.028	0.006	0.006	0.05	3.27
cis-2-butene	0.026	0.006	0.007	0.045	3.03
Aromatic					
toluene	0.523	0.361	0.035	2.82	38.34
benzene	0.286	0.112	0.032	0.742	20.97
m-xylene	0.123	0.237	0.015	3.579	9.02
ethyl benzene	0.107	0.134	0.017	2.052	7.84
o-xylene	0.103	0.214	0.015	3.294	7.55
OVOC					
acetone	3.297	0.835	0.412	5.978	52.47
acetaldehyde	1.742	0.635	0.276	5.805	27.73
methyl ethyl ketone	0.496	0.15	0.051	1.118	7.89
methyl t-butyl ether	0.213	0.208	0.018	1.512	3.39
propionaldehyde	0.178	0.081	0.028	0.572	2.83

19. Line 260: The wind speed during the campaign is low, so I would expect local emissions could have impacted the concentrations of the precursor species to a certain extent. 0.5 ppb isoprene was observed in the OCM sector (fig.2) which, to me, suggests some local influences which should be acknowledged.

Reply:

Thanks for your suggestion. We agree with the reviewer that YMK site is also

partially affected by emissions even during the OCM period. We acknowledge this in revised manuscript (Line 314-317).

Revision:

Line 314-317: Isoprene, a representative BVOC, achieved a diurnal concentration of 0.58 ± 0.06 ppb, indicated slightly local emissions could have impacted the concentrations of the precursor species even in OCM sector.

20. Line 319: In previous literature, e.g. Whalley et al., ACP, 2010, the inclusion of halogen chemistry led to an increase in modelled OH concentrations and a decrease in modelled HO2 concentration, so the decrease in the modelled OH concentration reported here is a little surprising – perhaps the differing levels of NOx between this study and RHaMBLe play a role? Could the authors provide a little more detail on the dominant reactions in the halogen scheme that are contributing to OH destruction?

Reply:

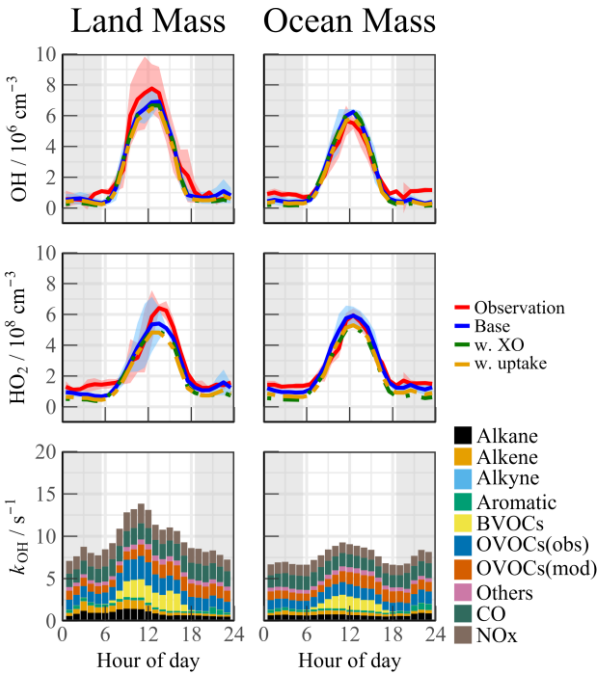

Fig. 4. Median diurnal profiles of the observed and modelled OH, HO_2, k_{OH} during LAM and OCM episodes. The coloured shadows for OH and HO_2 radicals denote the 25 and 75% percentiles. The grey areas denote nighttime.

Thanks for your suggestion. In order to better explore the effect of Br and I

chemistry on HOx radicals, we chose BrO/IO as the initiation point of halogen chemistry in the latest version of the manuscript. The concentration of BrO and IO is set to ~5 ppt, which is a typical level in MBL site (Xia et al., 2022; Bloss et al., 2010; Whalley et al., 2010). In this scenario (Fig. 4, green line). The daytime concentration of HO_2 radical decreased by 8.5% and 13.3% during the LAM and OCM periods, respectively, compared to the base model. However, there was no significant change in the concentration of OH radicals (<3%).

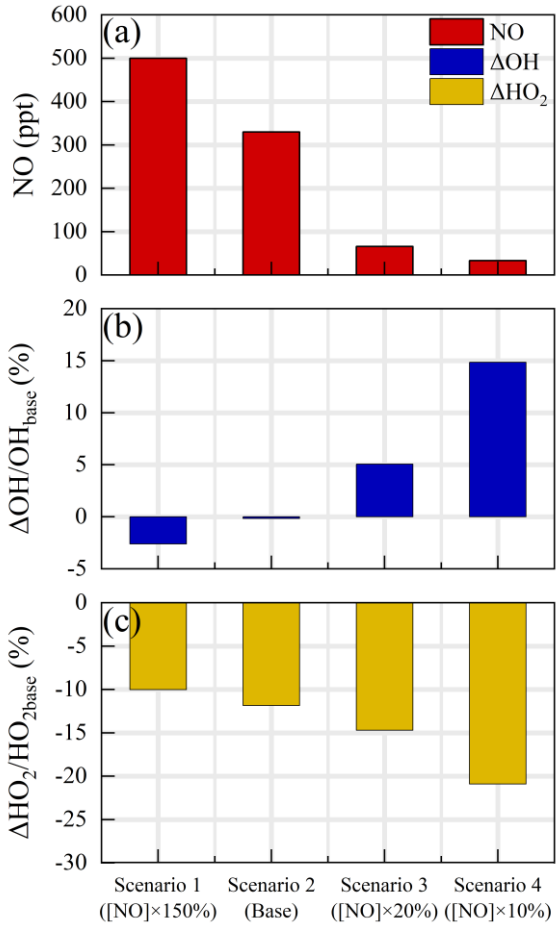

Fig. S6. By modifying the NO concentration in different levels (Scenario 1: [NO]×150%, Scenario 2: base, Scenario 3: [NO]×20%, Scenario 4: [NO]×10%), the response of HOx radicals to the halogen mechanism varied under different NO levels (30 – 500 ppt in the diurnal time).

Traditionally, it is believed that the inclusion of halogen chemistry leads to higher modeled OH concentrations and lower modeled HO_2 concentrations. Therefore, the lack of an increase in OH concentration with the introduction of the halogen mechanism at the YMK site calls for further investigation (Fig. S6). By modifying the NO concentration in different levels (Scenario 1: [NO]×150%, Scenario 2: base, Scenario 3: [NO]×20%, Scenario 4: [NO]×10%), the response of HOx radicals to the halogen

mechanism varied under different NO levels.

As the constrained NO increased from 30 ppt to 500 ppt, the reduction in HO_2 radicals due to the Br and I mechanisms ranged between 10% and 20%. At elevated NOx levels, reactions between halogen radicals and NOx occurred, inhibiting the formation of OH radicals. In Scenario 1, the OH concentration even decreased by 3.5% when introducing the halogen mechanism. When NO concentration was constrained around 30 ppt (Scenario 4), similar to those obtained in RHaMBLe/CYPHEX campaigns, the modelled OH concentration increased by 14.4%, while the HO_2 concentration decreased by approximately 20.8% (Whalley et al., 2010; Bloss et al., 2010). Therefore, the sensitivity of OH radicals to the halogen mechanism in the YMK region is primarily limited by the local NOx concentration level.

We have also made some changes in the manuscript (Line 417-442).

Revision:

Line 417-442: Halogen species have been recognized as potent oxidizers that can boost photochemistry (Xia et al., 2022; Peng et al., 2021). A sensitivity test was performed by imposing BrO and IO into the base model to diagnose the impact of the halogen chemistry on the troposphere chemistry. The concentration of BrO and IO is set to ~5 ppt, which is a typical level in MBL site (Xia et al., 2022; Bloss et al., 2010; Whalley et al., 2010). The details of the mechanisms involved are listed in Tables S3 and S4. In this scenario (Fig. 4, green line). The daytime concentration of HO_2 radical decreased by 8.5% and 13.3% during the LAM and OCM periods, respectively, compared to the base model. However, there was no significant change in the concentration of OH radicals (<3%). Traditionally, it is believed that the inclusion of halogen chemistry leads to higher modeled OH concentrations and lower modeled HO_2 concentrations. Therefore, the lack of an increase in OH concentration with the introduction of the halogen mechanism at the YMK site calls for further investigation (Fig. S6). By modifying the NO concentration in different levels (Scenario 1: [NO]×150%, Scenario 2: base, Scenario 3: [NO]×20%, Scenario 4: [NO]×10%), the response of HOx radicals to the halogen mechanism varied under different NO levels. As the constrained NO

increased from 30 ppt to 500 ppt, the reduction in HO_2 radicals due to the Br and I mechanisms ranged between 10% and 20%. At elevated NOx levels, reactions between halogen radicals and NOx occurred, inhibiting the formation of OH radicals. In Scenario 1, the OH concentration even decreased by 3.5% when introducing the halogen mechanism. When NO concentration was constrained around 30 ppt (Scenario 4), similar to those obtained in RHaMBLe/CYPHEX campaigns, the modelled OH concentration increased by 14.4%, while the HO_2 concentration decreased by approximately 20.8% (Whalley et al., 2010; Bloss et al., 2010). Therefore, the sensitivity of OH radicals to the halogen mechanism in the YMK region is primarily limited by the local NOx concentration level.

21. Fig. 4: This figure could be removed as figure 6 is more instructive.

Reply:

Thanks for your suggestion. We have removed the previous Fig.4.

22. Line 335 – 346: I'm not sure this case study adds anything to the paper as it stands and could be removed to make the paper more succinct.

Reply:

Thanks for your suggestion. The case and the previous Fig.5 have been removed to make the paper more succinct.

23. Line 358: I don't think the good agreement between modelled and measured HO2 should be used as an argument to exclude heterogeneous reactions in the model. If the inclusion of heterogeneous processes did reduce the modelled HO2 concentration, this could highlight missing HO2 sources in the model (or may indicate that some RO2 species present were detected as HO2) and so warrants investigation.

Reply:

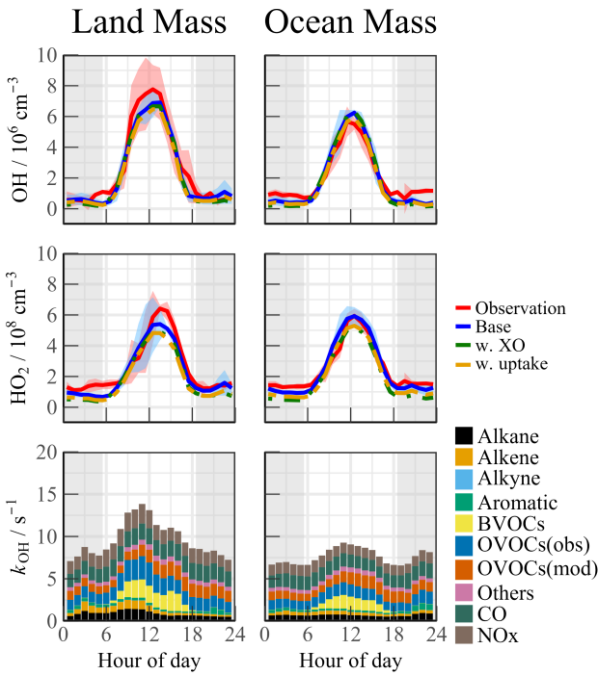

Fig. 4. Median diurnal profiles of the observed and modelled OH, HO_2, k_{OH} during LAM and OCM episodes. The coloured shadows for OH and HO_2 radicals denote the 25 and 75% percentiles. The grey areas denote nighttime.

Thanks for your suggestion. We agree with the reviewer that the good agreement between modelled and measured HO_2 should not be used as an argument to exclude heterogeneous reactions in the model. We have added the removal path of HO_2 radicals by heterogeneous uptake. The inclusion of heterogeneous processes (γ = 0.08) did reduce the modelled HO_2 concentration for ~10% during both LAM and OCM periods (Fig.4). This reduced agreement between observation and simulation emphasizes the presence of a missing HO_2 source in the base model.

Revision:

Line 277-289: The heterogeneous uptake of HO_2 is considered to play an important role in the MBL region (Whalley et al., 2010; Zou et al., 2022; Woodward-Massey et al., 2022). In order to assess the impact of HO_2 uptake on HOx radical chemistry, we incorporated HO_2 uptake reaction into the base model (Eq. (3) - (5)).

$$HO_2 + uptake \rightarrow products \quad (3)$$

$$k_{HO_2+uptake} = \frac{\gamma \times ASA \times v_{HO_2}}{k_{HO_2+NO}[NO]} \quad (4)$$

$$v_{HO_2} = \sqrt{\frac{8 \times R \times T}{0.033 \times \Pi}} \quad (5)$$

Here, ASA represents the aerosol surface area [$\mu m^2\ cm^{-3}$], which can be estimated as 20 times the $PM_{2.5}$ concentration [$\mu g/cm^3$]. ν_{HO_2} [cm^{-1}] can be calculated using Eq. (5), where T and R represent the temperature and gas constant, respectively. The heterogeneous uptake coefficien (γ) for HO_2 usually has high uncertainty, with typical values ranging from 0 to 1 (Song et al., 2021). In this study, we set γ to 0.08 to evaluate the influence of HO_2 uptake on radical concentrations.

Line 443-448: Alough the modelled and measured HO_2 showed good agreement，the effect of HO_2 heterogeneous processes on the chemistry of HOx radicals is also worth exploring. The inclusion of heterogeneous processes (γ = 0.08) did reduce the modelled HO_2 concentration for ~10% during both LAM and OCM periods (Fig. 4, yellow line). This reduced agreement between observation and simulation emphasizes the presence of a missing HO_2 source in the base model.

24. Line 371: Given the model slightly overestimates HO2 and the calculated OH reactivity could be an underestimate of the total OH reactivity actually present, a missing OH source may be masked. A comment on these points should be provided.

Reply:

Thanks for your suggestion. We added relevant comments on the missing OH sources.

Revision:

Line 404-405: Under enhanced photochemistry, the calculated OH reactivity could be an underestimation of the total OH reactivity, so a missing OH source may be masked.

25. Line 394: D(OH) should be considered a lower limit as it uses calculated rather than measured kOH. This should be made clear.

Reply:

Thanks for your suggestion. We emphasize this point in Line 467-470.

Revision:

Line 467-470: Because k_{OH} was not measured during the observation experiment, the simulated value was used to analyze the removal rate. Therefore, D(OH) should be considered a lower limit as it uses calculated rather than measured k_{OH} (Yang et al., 2022b).

26. Line 421 – 423: Again, following on from my earlier comments, without a measurement of kOH, the absence of unknown OH recycling pathways can't be confirmed here.

Reply:

Thanks for your suggestion. We modified the misleading description in Line 485-486.

Revision:

Line 485-486: When the simulated k_{OH} was introduced into the experimental budgets, the difference between P(OH) and D(OH) was less than 2 ppb/h.

27. Fig. 10, line 532 - 539: Some further details on how the model was run when it was used to predict ozone are needed. What model constraints were changed to variables other than ozone (presumably NO2 was also changed to a variable)? Why was the atmospheric lifetime changed from 18 hrs to 15 hrs and what was the rate of the first order loss term used? How did modelled OH, RO2 and HO2 change when the model was unconstrained to HONO?

Reply:

Thanks for your suggestion. When using the model to predict ozone, both O_3 and NO were changed to variables. The 15 hrs in the manuscript was a clerical mistake, and the atmospheric lifetime used in base model or ozone prediction was 18 hrs. Assuming a boundary layer height of about 1 km, the rate of the first order loss term at 18 hrs is about 1.5 cm/s. The modelled OH, HO_2 and RO_2 change when the model was unconstrained to HONO were shown in Fig.S7. After evaluation, in LAM and OCM

sectors, concentration changes for OH were 46.9% and 43.2%, for HO_2 were 38.3% and 34.3%, for RO_2 were 43.7% and 39.0%, respectively.

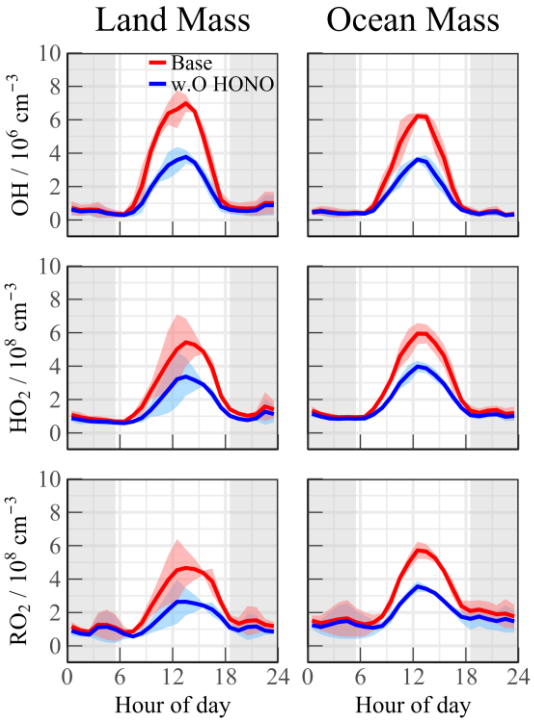

Fig. S7. The modelled OH, HO_2 and RO_2 change when the model was unconstrained to HONO during LAM and OCM sectors, respectively.

Revision:

Line 255-258: The physical losses of species due to processes such as deposition, convection, and advection were approximately replaced by an 18 h atmospheric lifetime, corresponding to first order loss rate of ~1.5 cm/s (by assuming a boundary layer height of about 1 km).

Line 604-605: On the basis of the base scenario run, constraints of the observed ozone and NO concentrations were removed to predict ozone.

Line 588-591: The modelled OH, HO_2 and RO_2 change when the model was unconstrained to HONO were shown in Fig. S7. After evaluation, in LAM and OCM sectors, concentration changes for OH were 46.9% and 43.2%, for HO_2 were 38.3% and 34.3%, for RO_2 were 43.7% and 39.0%, respectively.

28. ***Line 547 - 548: I'm not sure the findings from this study support this closing statement. Although the impact of HONO in this particular marine environment***

is interesting, the elevated HONO concentrations are somewhat of an anomaly compared to the other marine environments. In regions where HONO concentrations are elevated, the sources of HONO would need to be identified to aid pollution mitigation policies.

Reply:

Thank you for your suggestion. HONO measurements at the YMK site were conducted using a commercial Long-Path Absorption Photometer (LOPAP). The LOPAP method has been extensively tested for its suitability in detecting HONO in complex atmospheric conditions, as demonstrated in previous studies by (Yang et al., 2022a; Yang et al., 2021b; Wang et al., 2023). To ensure the accuracy of the measurements, zero air measurements were taken every 8 hours for a duration of 20 minutes to correct for instrument baseline fluctuations. This calibration procedure helps to minimize any potential biases and ensures the reliability of the HONO detection at the YMK site.

The high daytime HONO concentrations observed at the YMK site is a notable phenomenon. Given the location of the site, one possible contributor to the elevated HONO levels is emissions from cruise ships, as discussed in the study by (Sun et al., 2020). Additionally, other active tropospheric sources of HONO, such as heterogeneous reactions with NO_2 and photolysis of $p(NO_3^-)$ warrant consideration in the MBL area, as highlighted in the studies by (Zhu et al., 2022; Crilley et al., 2021).

29. Line 564 – 567: These statements need to be supported by evidence or removed.

Reply:

Thanks for your suggestion. These statements have been removed.

Minor Comments

1. ***Line 84: '..heterogeneous iodine-organic chemistry' Could the authors provide the specific reactions they are referring to here.***

Reply:

Thanks for your suggestion. (Huang et al., 2022) simulated the growth of particles with an aerosol model. The specific reactions considered in the model include Reactions as below:

$$IOP + H_2O \rightarrow HIO_3$$

$$HIO_3 + dimethylamine \rightarrow salt(low\ volatility/non-volatile)$$

$$glyoxal(or\ meso-erythritol) + HIO_3 \rightarrow organic\ acid(water\ soluble, low\ volatility)$$

$$organic\ acid + dimethylamine \rightarrow salt(non-volatile, stable\ salt)$$

2. ***Line 155: change 'avoid' to 'reduce'***

Reply:

Thanks for your suggestion. We have revised the manuscript as the reviewer's comment (Line 169).

3. ***Line 183-184: I'm not sure about the terminology used here 'conventional pollutants', 'secondary pollutant precursors' and 'destruction products'. I suggest just listing all these species and not attempting to categorise them.***

Reply:

Thanks for your suggestion. We have revised the manuscript as the reviewer's comment (Line 220-225).

4. ***Line 183: 'carbonic oxide' to 'carbon monoxide'***

Reply:

Thanks for your suggestion. We have revised the manuscript as the reviewer's comment (Line 223).

5. Line 198: change 'radical related secondary pollution' to 'ozone'

Reply:

Thanks for your suggestion. We have revised the manuscript as the reviewer's comment (Line 246).

6. Line 199: remove 'conventional'

Reply:

Thanks for your suggestion. We have revised the manuscript as the reviewer's comment (Line 248).

Revision:

The meteorological parameters, pollutants, and precursor concentrations mentioned in Section 2.2.2 were input into the model as boundary conditions.

7. Line 249: 'grooved distribution' is strange terminology, I would delete.

Reply:

Thanks for your suggestion. We have revised the manuscript as the reviewer's comment (Line 329-331).

8. Line 252: 'extremely high..' 'significantly affect..' need to be more specific.

Reply:

Thanks for your suggestion. We have revised the manuscript as the reviewer's comment (Line 333-334).

9. Line 277 – 278: This needs rewording, as it is written, it could be interpreted as meaning the ozone and HONO concentrations were higher during the OCM period.

Reply:

Thanks for your suggestion. We have deleted the misleading sentence.

10. Line 280: '..changed greatly' I would be explicit, i.e. T increased..From figure 2, J(O1D) is very similar between the two sectors.

Reply:

Thanks for your suggestion. We have revised the manuscript as the reviewer's comment (Line 323-324).

11. Line 360 -368: Suggest referencing section 4.1 here

Reply:

Thanks for your suggestion. We have revised the manuscript as the reviewer's comment (Line 390).

12. Line 448: 'loss' to 'production'

Reply:

Thanks for your suggestion. We have revised the manuscript as the reviewer's comment (Line 513).

13. Fig 11: The YMK campaign is labelled as STORM-II in this fig. Change to YMK for consistency.

Reply:

Thanks for your suggestion. We have changed the label to YMK for consistency.

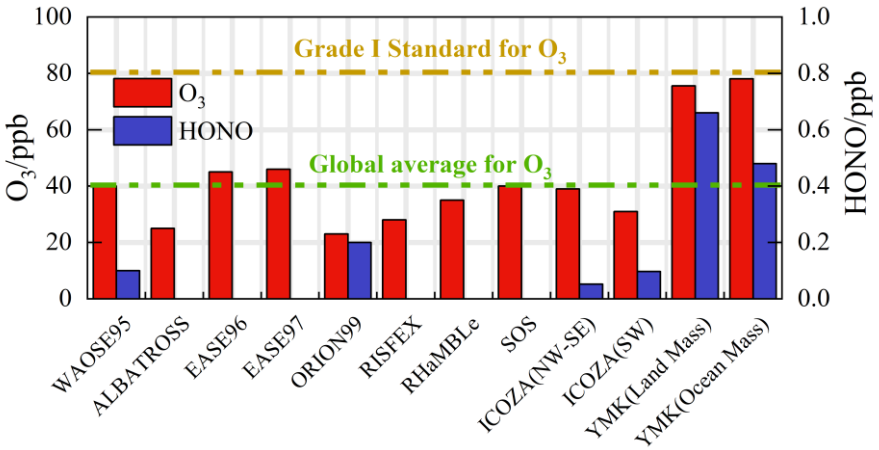

Reference

Atkinson, R., Baulch, D. L., Cox, R. A., Crowley, J. N., Hampson, R. F., Hynes, R. G., Jenkin, M. E., Rossi, M. J., and Troe, J.: Evaluated kinetic and photochemical data for atmospheric chemistry: Volume III - gas phase reactions of inorganic halogens, Atmos Chem Phys, 7, 981-1191, 10.5194/acp-7-981-2007, 2007.

Bloss, W. J., Rowley, D. M., Cox, R. A., and Jones, R. L.: Kinetics and products of the IO self-reaction, J Phys Chem A, 105, 7840-7854, 10.1021/jp0044936, 2001.

Bloss, W. J., Camredon, M., Lee, J. D., Heard, D. E., Plane, J. M. C., Saiz-Lopez, A., Bauguitte, S. J. B., Salmon, R. A., and Jones, A. E.: Coupling of HOx, NOx and halogen chemistry in the antarctic boundary layer, Atmos Chem Phys, 10, 10187-10209, 10.5194/acp-10-10187-2010, 2010.

Cox, R. A., Bloss, W. J., Jones, R. L., and Rowley, D. M.: OIO and the atmospheric cycle of iodine, Geophys Res Lett, 26, 1857-1860, 10.1029/1999gl900439, 1999.

Crilley, L. R., Kramer, L. J., Pope, F. D., Reed, C., Lee, J. D., Carpenter, L. J., Hollis, L. D. J., Ball, S. M., and Bloss, W. J.: Is the ocean surface a source of nitrous acid (HONO) in the marine boundary layer?, Atmos Chem Phys, 21, 18213-18225, 10.5194/acp-21-18213-2021, 2021.

Dillon, T. J., Tucceri, M. E., and Crowley, J. N.: Laser induced fluorescence studies of iodine oxide chemistry Part II. The reactions of IO with CH3O2, CF3O2 and O-3, Phys Chem Chem Phys, 8, 5185-5198, 10.1039/b611116e, 2006.

Enami, S., Yamanaka, T., Nakayama, T., Hashimoto, S., Kawasaki, M., Shallcross, D. E., Nakano, Y., and Ishiwata, T.: A gas-phase kinetic study of the reaction between bromine monoxide and methylperoxy radicals at atmospheric temperatures, J Phys Chem A, 111, 3342-3348, 10.1021/jp068390k, 2007.

Fuchs, H., Tan, Z., Hofzumahaus, A., Broch, S., Dorn, H.-P., Holland, F., Kuenstler, C., Gomm, S., Rohrer, F., Schrade, S., Tillmann, R., and Wahner, A.: Investigation of potential interferences in the detection of atmospheric ROx radicals by laser-induced fluorescence under dark conditions, Atmos Meas Tech, 9, 1431-1447, 10.5194/amt-9-1431-2016, 2016.

Fuchs, H., Tan, Z., Lu, K., Bohn, B., Broch, S., Brown, S. S., Dong, H., Gomm, S., Haeseler, R., He, L., Hofzumahaus, A., Holland, F., Li, X., Liu, Y., Lu, S., Min, K.-E., Rohrer, F., Shao, M., Wang, B., Wang, M., Wu, Y., Zeng, L., Zhang, Y., Wahner, A., and Zhang, Y.: OH reactivity at a rural site (Wangdu) in the North China Plain: contributions from OH reactants and experimental OH budget, Atmos Chem Phys, 17, 645-661, 10.5194/acp-17-645-2017, 2017.

Griffith, S. M., Hansen, R. F., Dusanter, S., Michoud, V., Gilman, J. B., Kuster, W. C., Veres, P. R., Graus, M., de Gouw, J. A., Roberts, J., Young, C., Washenfelder, R., Brown, S. S., Thalman, R., Waxman, E., Volkamer, R., Tsai, C., Stutz, J., Flynn, J. H., Grossberg, N., Lefer, B., Alvarez, S. L., Rappenglueck, B., Mielke, L. H., Osthoff, H. D., and Stevens, P. S.: Measurements of hydroxyl and hydroperoxy radicals during CalNex-LA: Model comparisons and radical budgets, J Geophys Res-Atmos, 121, 4211-4232, 10.1002/2015jd024358, 2016.

Huang, R. J., Hoffmann, T., Ovadnevaite, J., Laaksonen, A., Kokkola, H., Xu, W., Xu, W., Ceburnis, D., Zhang, R., Seinfeld, J. H., and O'Dowd, C.: Heterogeneous iodine-organic chemistry fast-tracks marine new particle formation, Proc Natl Acad Sci U S A, 119, e2201729119, 10.1073/pnas.2201729119, 2022.

Jiang, Y., Xue, L., Shen, H., Dong, C., Xiao, Z., and Wang, W.: Dominant Processes of HONO Derived from Multiple Field Observations in Contrasting Environments, Environmental Science & Technology Letters, 10.1021/acs.estlett.2c00004, 2022.

Joseph, D. M., Ashworth, S. H., and Plane, J. M. C.: On the photochemistry of IONO2: absorption cross

section (240-370 nm) and photolysis product yields at 248 nm, Phys Chem Chem Phys, 9, 5599-5607, 10.1039/b709465e, 2007.
Kaltsoyannis, N. and Plane, J. M. C.: Quantum chemical calculations on a selection of iodine containing species (IO, OIO, INO3, (IO)(2), I2O3, I2O4 and I2O5) of importance in the atmosphere (vol 10, pg 1723, 2008), Phys Chem Chem Phys, 10, 7329-7329, 2008.
Li, X., Rohrer, F., Brauers, T., Hofzumahaus, A., Lu, K., Shao, M., Zhang, Y. H., and Wahner, A.: Modeling of HCHO and CHOCHO at a semi-rural site in southern China during the PRIDE-PRD2006 campaign, Atmos Chem Phys, 14, 12291-12305, 10.5194/acp-14-12291-2014, 2014.
Lu, K. D., Rohrer, F., Holland, F., Fuchs, H., Bohn, B., Brauers, T., Chang, C. C., Haeseler, R., Hu, M., Kita, K., Kondo, Y., Li, X., Lou, S. R., Nehr, S., Shao, M., Zeng, L. M., Wahner, A., Zhang, Y. H., and Hofzumahaus, A.: Observation and modelling of OH and HO2 concentrations in the Pearl River Delta 2006: a missing OH source in a VOC rich atmosphere, Atmos Chem Phys, 12, 1541-1569, 10.5194/acp-12-1541-2012, 2012.
Ma, X., Tan, Z., Lu, K., Yang, X., Chen, X., Wang, H., Chen, S., Fang, X., Li, S., Li, X., Liu, J., Liu, Y., Lou, S., Qiu, W., Wang, H., Zeng, L., and Zhang, Y.: OH and HO2 radical chemistry at a suburban site during the EXPLORE-YRD campaign in 2018, Atmos Chem Phys, 22, 7005-7028, 10.5194/acp-22-7005-2022, 2022.
Mao, J., Ren, X., Chen, S., Brune, W. H., Chen, Z., Martinez, M., Harder, H., Lefer, B., Rappenglück, B., Flynn, J., and Leuchner, M.: Atmospheric oxidation capacity in the summer of Houston 2006: Comparison with summer measurements in other metropolitan studies, Atmos Environ, 44, 4107-4115, 10.1016/j.atmosenv.2009.01.013, 2010.
Martin, J. C. G., Ashworth, S. H., Mahajan, A. S., and Plane, J. M. C.: Photochemistry of OIO: Laboratory study and atmospheric implications, Geophys Res Lett, 36, 10.1029/2009gl037642, 2009.
Niu, Y. B., Zhu, B., He, L. Y., Wang, Z., Lin, X. Y., Tang, M. X., and Huang, X. F.: Fast Nocturnal Heterogeneous Chemistry in a Coastal Background Atmosphere and Its Implications for Daytime Photochemistry, Journal of Geophysical Research: Atmospheres, 127, 10.1029/2022jd036716, 2022.
Novelli, A., Hens, K., Ernest, C. T., Kubistin, D., Regelin, E., Elste, T., Plass-Duelmer, C., Martinez, M., Lelieveld, J., and Harder, H.: Characterisation of an inlet pre-injector laser-induced fluorescence instrument for the measurement of atmospheric hydroxyl radicals, Atmos Meas Tech, 7, 3413-3430, 10.5194/amt-7-3413-2014, 2014.
Orlando, J. J. and Tyndall, G. S.: Rate coefficients for the thermal decomposition of BrONO2 and the heat of formation of BrONO2, J Phys Chem-Us, 100, 19398-19405, 10.1021/jp9620274, 1996.
Peng, X., Wang, W. H., Xia, M., Chen, H., Ravishankara, A. R., Li, Q. Y., Saiz-Lopez, A., Liu, P. F., Zhang, F., Zhang, C. L., Xue, L. K., Wang, X. F., George, C., Wang, J. H., Mu, Y. J., Chen, J. M., and Wang, T.: An unexpected large continental source of reactive bromine and chlorine with significant impact on wintertime air quality, Natl. Sci. Rev., 8, 10.1093/nsr/nwaa304, 2021.
Plane, J. M. C., Joseph, D. M., Allan, B. J., Ashworth, S. H., and Francisco, J. S.: An experimental and theoretical study of the reactions OIO plus NO and OH plus OH, J Phys Chem A, 110, 93-100, 10.1021/jp055364y, 2006.
Saunders, R. W. and Plane, J. M. C.: Formation pathways and composition of iodine oxide ultra-fine particles, Environmental Chemistry, 2, 299-303, 10.1071/en05079, 2005.
Slater, E. J., Whalley, L. K., Woodward-Massey, R., Ye, C., Lee, J. D., Squires, F., Hopkins, J. R., Dunmore, R. E., Shaw, M., Hamilton, J. F., Lewis, A. C., Crilley, L. R., Kramer, L., Bloss, W., Vu, T., Sun, Y., Xu, W., Yue, S., Ren, L., Acton, W. J. F., Hewitt, C. N., Wang, X., Fu, P., and Heard, D. E.:

Elevated levels of OH observed in haze events during wintertime in central Beijing, Atmos Chem Phys, 20, 14847-14871, 10.5194/acp-20-14847-2020, 2020.
Song, H., Lu, K., Dong, H., Tan, Z., Chen, S., Zeng, L., and Zhang, Y.: Reduced Aerosol Uptake of Hydroperoxyl Radical May Increase the Sensitivity of Ozone Production to Volatile Organic Compounds, Environmental Science & Technology Letters, 9, 22-29, 10.1021/acs.estlett.1c00893, 2021.
Sun, L., Chen, T., Jiang, Y., Zhou, Y., Sheng, L., Lin, J., Li, J., Dong, C., Wang, C., Wang, X., Zhang, Q., Wang, W., and Xue, L.: Ship emission of nitrous acid (HONO) and its impacts on the marine atmospheric oxidation chemistry, Sci Total Environ, 735, 139355, 10.1016/j.scitotenv.2020.139355, 2020.
Tan, Z. F., Lu, K. D., Hofzumahaus, A., Fuchs, H., Bohn, B., Holland, F., Liu, Y. H., Rohrer, F., Shao, M., Sun, K., Wu, Y. S., Zeng, L. M., Zhang, Y. S., Zou, Q., Kiendler-Scharr, A., Wahner, A., and Zhang, Y. H.: Experimental budgets of OH, HO2, and RO2 radicals and implications for ozone formation in the Pearl River Delta in China 2014, Atmos Chem Phys, 19, 7129-7150, 10.5194/acp-19-7129-2019, 2019.
Wang, F., Hu, R., Xie, P., Wang, Y., Chen, H., Zhang, G., and Liu, W.: Calibration source for OH radical based on synchronous photolysis, Acta Phys Sin-Ch Ed, 69, 2020.
Wang, F. Y., Hu, R. Z., Chen, H., Xie, P. H., Wang, Y. H., Li, Z. Y., Jin, H. W., Liu, J. G., and Liu, W. Q.: Development of a field system for measurement of tropospheric OH radical using laser-induced fluorescence technique, Opt. Express, 27, A419-A435, 10.1364/oe.27.00a419, 2019.
Wang, J., Zhang, Y., Zhang, C., Wang, Y., Zhou, J., Whalley, L. K., Slater, E. J., Dyson, J. E., Xu, W., Cheng, P., Han, B., Wang, L., Yu, X., Wang, Y., Woodward-Massey, R., Lin, W., Zhao, W., Zeng, L., Ma, Z., Heard, D. E., and Ye, C.: Validating HONO as an Intermediate Tracer of the External Cycling of Reactive Nitrogen in the Background Atmosphere, Environ Sci Technol, 10.1021/acs.est.2c06731, 2023.
Wang, Y., Hu, R., Xie, P., Chen, H., Wang, F., Liu, X., Liu, J., and Liu, W.: Measurement of tropospheric HO2 radical using fluorescence assay by gas expansion with low interferences, J Environ Sci (China), 99, 40-50, 10.1016/j.jes.2020.06.010, 2021.
Whalley, L. K., Furneaux, K. L., Goddard, A., Lee, J. D., Mahajan, A., Oetjen, H., Read, K. A., Kaaden, N., Carpenter, L. J., Lewis, A. C., Plane, J. M. C., Saltzman, E. S., Wiedensohler, A., and Heard, D. E.: The chemistry of OH and HO2 radicals in the boundary layer over the tropical Atlantic Ocean, Atmos Chem Phys, 10, 1555-1576, 2010.
Whalley, L. K., Slater, E. J., Woodward-Massey, R., Ye, C., Lee, J. D., Squires, F., Hopkins, J. R., Dunmore, R. E., Shaw, M., Hamilton, J. F., Lewis, A. C., Mehra, A., Worrall, S. D., Bacak, A., Bannan, T. J., Coe, H., Percival, C. J., Ouyang, B., Jones, R. L., Crilley, L. R., Kramer, L. J., Bloss, W. J., Vu, T., Kotthaus, S., Grimmond, S., Sun, Y., Xu, W., Yue, S., Ren, L., Acton, W. J. F., Hewitt, C. N., Wang, X., Fu, P., and Heard, D. E.: Evaluating the sensitivity of radical chemistry and ozone formation to ambient VOCs and NOx in Beijing, Atmos Chem Phys, 21, 2125-2147, 10.5194/acp-21-2125-2021, 2021.
Woodward-Massey, R., Sommariva, R., Whalley, L. K., Cryer, D. R., Ingham, T., Bloss, W. J., Ball, S. M., Lee, J. D., Reed, C. P., Crilley, L. R., Kramer, L. J., Bandy, B. J., Forster, G. L., Reeves, C. E., Monks, P. S., and Heard, D. E.: Radical chemistry at a UK coastal receptor site – Part 1: observations of OH, HO2, RO2, and OH reactivity and comparison to MCM model predictions, Atmos. Chem. Phys., 10.5194/acp-2022-207, 2022.
Xia, M., Wang, T., Wang, Z., Chen, Y., Peng, X., Huo, Y., Wang, W., Yuan, Q., Jiang, Y., Guo, H., Lau, C., Leung, K., Yu, A., and Lee, S.: Pollution-Derived Br2 Boosts Oxidation Power of the Coastal Atmosphere, Environ Sci Technol, 10.1021/acs.est.2c02434, 2022.
Yang, X., Lu, K., Ma, X., Gao, Y., Tan, Z., Wang, H., Chen, X., Li, X., Huang, X., He, L., Tang, M., Zhu, B., Chen, S., Dong, H., Zeng, L., and Zhang, Y.: Radical chemistry in the Pearl River Delta: observations

and modeling of OH and HO2 radicals in Shenzhen in 2018, Atmos Chem Phys, 22, 12525-12542, 10.5194/acp-22-12525-2022, 2022a.
Yang, X., Lu, K., Ma, X., Gao, Y., Tan, Z., Wang, H., Chen, X., Li, X., Huang, X., He, L., Tang, M., Zhu, B., Chen, S., Dong, H., Zeng, L., and Zhang, Y.: Radical chemistry in the Pearl River Delta: observations and 2 modeling of OH and HO2 radicals in Shenzhen 2018, 10.5194/acp-2022-113, 2022b.
Yang, X., Lu, K., Ma, X., Liu, Y., Wang, H., Hu, R., Li, X., Lou, S., Chen, S., Dong, H., Wang, F., Wang, Y., Zhang, G., Li, S., Yang, S., Yang, Y., Kuang, C., Tan, Z., Chen, X., Qiu, P., Zeng, L., Xie, P., and Zhang, Y.: Observations and modeling of OH and HO2 radicals in Chengdu, China in summer 2019, The Science of the total environment, 772, 144829-144829, 10.1016/j.scitotenv.2020.144829, 2021a.
Yang, Y., Li, X., Zu, K., Lian, C., Chen, S., Dong, H., Feng, M., Liu, H., Liu, J., Lu, K., Lu, S., Ma, X., Song, D., Wang, W., Yang, S., Yang, X., Yu, X., Zhu, Y., Zeng, L., Tan, Q., and Zhang, Y.: Elucidating the effect of HONO on O3 pollution by a case study in southwest China, Sci Total Environ, 756, 144127, 10.1016/j.scitotenv.2020.144127, 2021b.
Zhang, G., Hu, R., Xie, P., Lu, K., Lou, S., Liu, X., Li, X., Wang, F., Wang, Y., Yang, X., Cai, H., Wang, Y., and Liu, W.: Intercomparison of OH radical measurement in a complex atmosphere in Chengdu, China, Sci Total Environ, 155924, 10.1016/j.scitotenv.2022.155924, 2022.
Zhu, B., Huang, X.-F., Xia, S.-Y., Lin, L.-L., Cheng, Y., and He, L.-Y.: Biomass-burning emissions could significantly enhance the atmospheric oxidizing capacity in continental air pollution, Environ. Pollut., 285, 10.1016/j.envpol.2021.117523, 2021.
Zhu, Y., Wang, Y., Zhou, X., Elshorbany, Y. F., Ye, C., Hayden, M., and Peters, A. J.: An investigation into the chemistry of HONO in the marine boundary layer at Tudor Hill Marine Atmospheric Observatory in Bermuda, Atmos Chem Phys, 22, 6327-6346, 10.5194/acp-22-6327-2022, 2022.
Zou, Z., Chen, Q., Xia, M., Yuan, Q., Chen, Y., Wang, Y., Xiong, E., Wang, Z., and Wang, T.: OH measurements in the coastal atmosphere of South China: missing OH sinks in aged air masses, EGUsphere, 2022, 1-47, 10.5194/egusphere-2022-854, 2022.